



Waveguide efficient directional coupling and decoupling via an integrated plasmonic nanoantenna

GUILLAUME BLANQUER,¹ VIVIEN LOO,¹ NANCY RAHBANY,¹
CHRISTOPHE COUTEAU,²  SYLVAIN BLAIZE,² RAFAEL
SALAS-MONTIEL,²  YANNICK DE WILDE,¹  AND VALENTINA
KRACHMALNICOFF^{1,*}

¹*Institut Langevin, ESPCI Paris, Université PSL, CNRS, 75005 Paris, France*

²*Laboratory Light, Nanomaterials & Nanotechnologies – L2n, University of Technology of Troyes (UTT) & CNRS ERL 7004, 12 rue Marie Curie, Troyes, France*

**valentina.krachmalnicoff@espci.fr*

Abstract: The development of integrated photonic devices has led to important advancements in the field of light-matter interaction at the nanoscale. One of the main focal points is the coupling between single photon emitters and optical waveguides aiming to achieve efficient optical confinement and propagation. In this work, we focus on the characterization of a hybrid dielectric/plasmonic waveguide consisting of a gold triangular nanoantenna placed on top of a TiO₂ waveguide. The strong directionality of the device is experimentally demonstrated by comparing the intensity scattered by the nanotriangle to the one scattered by a SNOM tip for different illumination geometries. The ability of the plasmonic antenna to generate powerful coupling between a single emitter and the waveguide will also be highlighted through numerical simulations.

© 2021 Optical Society of America under the terms of the [OSA Open Access Publishing Agreement](#)

1. Introduction

The development of integrated optical devices has promoted significant advancement in controlling light-matter interaction at the nanoscale. Such opto-electronic devices aim to perform and implement logical operations using optical components [1], which has led to a decrease in their size reaching a limit that conventional electronic circuits cannot endure. This is particularly promising, as technological and physical limits hamper the improvement of the computing capacities of conventional electronic processors, a problem that is overcome by integrated photonic devices [2]. Another advantage is their low energy consumption and low cross-talk compared to microelectronic devices [3]. In addition, integrated photonic circuits have important applications in the field of quantum optics and quantum information processing [4–8]. The main building blocks of quantum photonic circuits are single photon sources [9,10]. The development of such new technologies lies in the effective coupling of the light emitted by single emitters into optical waveguides, as well as the efficient communication between them [11,12]. An enhanced coupling of a single emitter to its environment can be achieved thanks to the use of plasmonic structures. The latter offer the advantage of strong field confinement and support surface plasmon polaritons (SPPs) with propagation lengths of several micrometers in the visible range. SPP-assisted energy transfer between emitters located up to 10 μm apart has been demonstrated on fully metallic SPP waveguides [13,14]. Such devices produce a strong attenuation of SPPs due to ohmic losses in the metal, which limits the communication distance between emitter and receiver and its efficiency. It was shown that hybrid structures comprising optical waveguides and embedded nanoantennas could be useful in overcoming this problem. Integrating a triangular nanoantenna on an optical waveguide demonstrated strong electromagnetic confinement at the

apex of the triangle [15–17], and enhanced photoluminescence of emitters [18]. V-shaped nanoantennas placed on dielectric waveguides showed strong directivity [19–21], and significant influence on the far-field emission diagram of fluorescent emitters [22], and both an efficient coupling and a strong directionality was achieved with Yagi-Uda nanoantennas made of gold nanorods integrated on dielectric waveguides [23]. Regarding the possibility to position precisely fluorescent dipole emitters at specific locations on a photonic integrated circuit, besides the manipulation of active fluorescent probes with a scanning probe microscope [24,25], it has been recently shown that direct laser writing based on two-photon polymerization is an attractive novel method to integrate nanoemitters in a controlled manner on optical glass waveguides [26], and that it can benefit from the hot spots formed around plasmonic nanostructures [27].

In this work, we develop a device made up of a hybrid nanoantenna/dielectric waveguide (DWG) aiming to couple the light emitted by a single photon source and potentially achieve efficient communication with a distant receiver. We choose a system consisting of a triangular gold nanoantenna deposited on a titanium dioxide (TiO_2) DWG. The advantage of the dielectric nature of the waveguide is that it allows light propagation to distances much greater than those provided by SPPs. In addition, the aim of the plasmonic nanoantenna, triangular shaped, is to improve the coupling between the emitter and the DWG, and to provide strong directionality of the coupled light with an easy to fabricate device with respect to more complex geometries.

Directionality is due indeed to mode matching at the base of the nanotriangle [17]. The mode propagating in the DWG excites hybrid plasmonic–photonic modes at the base of the nanotriangle. The electromagnetic energy is exchanged between the plasmonic mode in the nanotriangle and the photonic modes propagating in the DWG. The resulting mode becomes a predominantly-plasmonic mode. Due to the narrowing of the gold layer from the base to the apex of the triangle, this mode is concentrated at the nanotriangle's apex giving rise to a directional phenomenon. Changing the dimensions of the triangle will modify the coupling from and to the DWG.

Furthermore, placing two distant similar nanotriangles base-to-base on the DWG will allow to inject and decouple the confined light, achieving energy transfer from the emitter to the receiver via the DWG.

2. Experimental results

Our hybrid structure was fabricated by a two-step electron beam lithography (EBL) technique. We first start by fabricating the DWGs made of TiO_2 (length = 30 μm , width = 1 μm) on a glass substrate (e-beam dose = 140 pC cm^{-2}). After the EBL process, a 150 nm layer of TiO_2 is evaporated. The DWGs are slanted at their ends to avoid any Fabry-Pérot effect. The second more critical step involves the exact positioning of the triangular gold nanoantennas at the center of the DWGs. After ensuring perfect alignment of the DWGs, triangular regions of 500 nm base and 500 nm height are insulated in the EBL polymer (e-beam dose = 300 pC cm^{-2}). Then, a 30 nm layer of SiO_2 is evaporated, followed by a 50 nm layer of gold. The SiO_2 spacer is added to provide better index matching between the triangles and the DWGs and ensure better coupling [15,16]. In Fig. 1, we show an optical image of the fabricated hybrid nanoantenna/DWG structures (a), as well as scanning electron microscope (SEM) images of double nanotriangles placed base-to-base on the DWG (b), and a single nanotriangle placed in the center of the DWG (c).

The strong directivity of the hybrid structure, comprising a single triangular nanoantenna, is demonstrated experimentally by measuring the decoupling efficiency as a function of the direction of light propagation in the DWG. Due to the asymmetric shape of the plasmonic triangular nanoantenna, we expect two different values of the decoupling efficiency. In order to characterize the directionality of the nanoantenna, we perform two measurements of the scattered intensity (using an EMCCD), corresponding to light propagating in the DWG from the base side to the

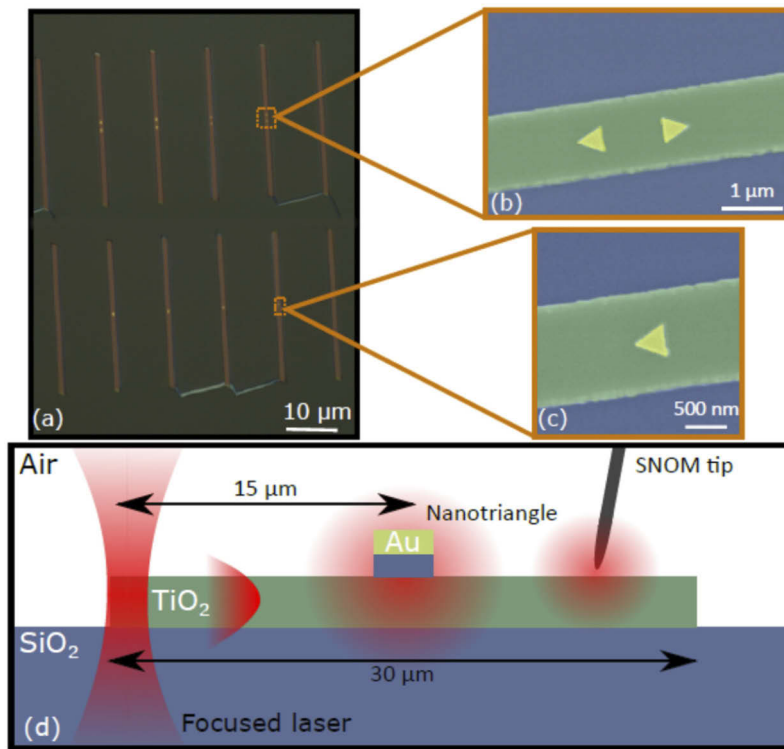


Fig. 1. (a) Optical image of the hybrid nanoantenna/DWG structures. Scanning Electron Microscope (SEM) images of (b) two nanotriangles placed base-to-base on the DWG, and (c) a single nanotriangle placed in the center of the DWG (false colors). (d) Sketch of the sample, the illumination geometry, and the SNOM tip. The light scattered by the nanotriangle and the SNOM tip is imaged on an EM-CCD camera.

apex side of the triangle and vice-versa. As shown in Fig. 1(d), we illuminate the DWG extremity by a focused laser beam beneath the sample. A portion of the incident light couples into the DWG and propagates towards the triangular nanoantenna where it decouples and scatters into the far-field. The comparison between the intensity scattered by the antenna in the two propagation directions is crucially related to the repeatability of the experiment. The two cases are studied independently and therefore we cannot guarantee the exact same coupling of the laser in the DWG from both sides. Indeed, such coupling is affected by several hard to control parameters such as the position of the laser spot on the extremity of the DWG, the position of the focal plane with respect to the DWG and the roughness of its slanted ends. In addition, we are forced to move the sample and realign it whenever we want to change the illumination side of the DWG in the experiments.

In order to circumvent this problem, we compare the intensity of guided light scattered by the nanoantenna to the intensity scattered by a chemically-etched tungsten SNOM tip placed on the DWG. This results in four independent cases illustrated in Figs. 2 (a)-2(d). For light propagating from the extremity of the DWG towards the base of the nanotriangle, the SNOM tip is placed either on the base-side (Fig. 2(a)) or the apex-side of the triangle (Fig. 2(b)). Similarly, for light propagating from the extremity of the DWG towards the apex of the nanotriangle, the SNOM tip is placed either on the apex-side (Fig. 2(c)) or the base-side of the triangle (Fig. 2(d)). We then extract the scattered intensity for both the nanoantenna and the SNOM tip which we utilize here as a reference.

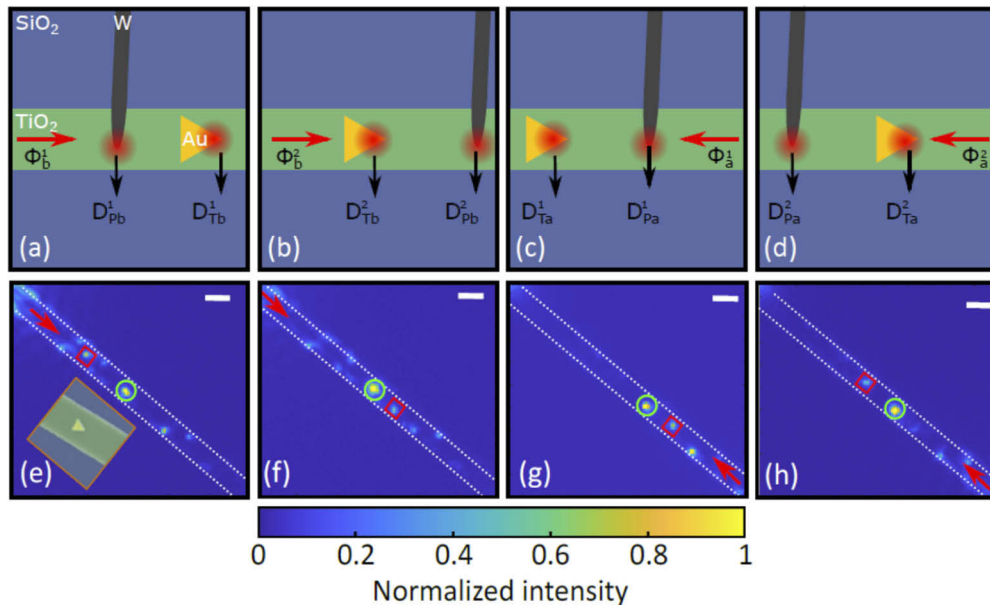


Fig. 2. (a) – (d) Sketches of the four different cases studied for characterizing the hybrid DWG. The direction of light propagation is indicated by the red arrow. For light propagating from the extremity of the DWG towards the base of the nanotriangle, the SNOM tip is placed on the DWG either (a) on the base-side, or (b) on the apex-side of the triangle. For light propagating from the extremity of the DWG towards the apex of the nanotriangle, the SNOM tip is placed on the DWG either (c) on the apex-side, or (d) on the base-side of the triangle. (e) – (f) Intensity maps corresponding to the four cases (a) – (d). Red squares represent the zones where the SNOM tip was displaced. Green circles represent the position of the nanoantenna on the DWG. White scale bars correspond to 1 μm .

To detail more, a laser of wavelength 600 nm is focused on the extremity of the DWG so that a fraction of the incident light is coupled to the DWG and propagates towards the nanotriangle as shown in Fig. 1(d). We use an EMCCD Peltier cooled highly sensitive camera to image the sample through a microscope oil objective (100x, NA = 1.43), to finely adjust the position of the SNOM tip at the top of the DWG and to perform high sensitivity measurements of the intensity of the light scattered by the SNOM tip and the nanotriangles. For each configuration sketched in Figs. 2 (a)-2(d), the SNOM tip is placed at the center of the DWG and scans a region of $600 \times 600 \text{ nm}^2$ by steps of 75 nm, where each scanning line perpendicular to the waveguide axis is scanned twice (back and forth). For each measurement point, an image is recorded via the EMCCD with an integration time of 10 s. This results in 128 images being recorded in every configuration. One of the 128 images is shown for each configuration in Figs. 2 (e) – 2(h). The zones where the SNOM tip was displaced are delimited by the red squares and the position of the nanoantenna on the DWG by green circles. Intensity hot spots on the edge of the waveguide are also visible. These hot spots are induced by defects that occurred during the manufacture of the sample.

3. Decoupling efficiency model

To calculate the decoupling efficiency values from the nanoantenna and the SNOM tip as a function of the light propagation direction, we use the fact that the scattering efficiency of the SNOM tip is constant at any position along the DWG. As shown in Figs. 2(e)-2(h), losses in the portion of the DWG between the tip and the nanotriangle are negligible with respect to the light

scattered by the antenna and the tip. We also assume that the tip and the nanotriangle scatter the same modes of the propagating light in the DWG as verified by numerical simulations. Based on these facts, we can now build a simple model to determine the decoupling efficiency values based on the scattered intensity measurements of both scatterers.

3.1. Light propagating towards the base of the nanotriangle

Let us consider first the case in which the light propagates from one extremity of the DWG towards the base of the nanotriangle. When the SNOM tip is placed on the base-side (Fig. 2(a)), the intensity scattered by the SNOM tip is defined as:

$$D_{Pb} = \gamma_{Pb}\phi_b, \quad (1)$$

where ϕ_b is the intensity of the light propagating in the DWG and γ_{Pb} is the decoupling coefficient of the SNOM tip.

The intensity scattered by the nanotriangle is:

$$D_{Tb} = (1 - \gamma_{Pb})\gamma_b\phi_b \quad (2)$$

where γ_b is the decoupling coefficient of the nanotriangle.

Similarly, when the SNOM tip is placed on the nanotriangle's apex-side (Fig. 2(b)), the intensity scattered by the nanotriangle is:

$$\tilde{D}_{Tb} = \gamma_b\tilde{\phi}_b \quad (3)$$

and the intensity scattered by the SNOM tip is:

$$\tilde{D}_{Pb} = (1 - \gamma_b)\gamma_{Pb}\tilde{\phi}_b \quad (4)$$

where $\tilde{\phi}_b$ is the intensity of the light propagating in the DWG.

Therefore, the decoupling coefficients of the SNOM tip and the nanotriangle can be expressed as:

$$\gamma_{Pb} = \frac{\chi_b - 1}{\chi_b + \frac{\tilde{D}_{Tb}}{\tilde{D}_{Pb}}} \quad \text{and} \quad \gamma_b = \frac{\chi_b - 1}{\chi_b + \frac{D_{Pb}}{D_{Tb}}} \quad (5)$$

where $\chi_b = \frac{D_{Pb}\tilde{D}_{Tb}}{D_{Tb}\tilde{D}_{Pb}}$.

3.2. Light propagating towards the apex of the nanotriangle

We can write analogue equations to describe the case in which light propagates from the extremity of the DWG towards the apex of the nanotriangle. One ends up with the following expressions for the decoupling coefficient of the SNOM tip γ_{Pa} and the decoupling coefficient of the nanotriangle γ_a :

$$\gamma_{Pa} = \frac{\chi_a - 1}{\chi_a + \frac{\tilde{D}_{Ta}}{\tilde{D}_{Pa}}} \quad \text{and} \quad \gamma_a = \frac{\chi_a - 1}{\chi_a + \frac{D_{Pa}}{D_{Ta}}} \quad (6)$$

where $\chi_a = \frac{D_{Pa}\tilde{D}_{Ta}}{D_{Ta}\tilde{D}_{Pa}}$. For the case in which the SNOM tip is placed on the side of the apex (Fig. 2(c)), $D_{Pa} = \gamma_{Pa}\phi_a$ is the intensity scattered by the tip and $D_{Ta} = (1 - \gamma_{Pa})\gamma_a\phi_a$ is the intensity scattered by the nanotriangle, with ϕ_a being the intensity of the light propagating in the DWG. Similarly, when the SNOM tip is placed on the side of the base of the nanotriangle (Fig. 2(d)), $\tilde{D}_{Pa} = (1 - \gamma_a)\gamma_{Pa}\tilde{\phi}_a$ is the intensity scattered by the tip and $\tilde{D}_{Ta} = \gamma_a\tilde{\phi}_a$ is the intensity scattered by the nanotriangle.

3.3. Decoupling efficiency measurements

The decoupling coefficients can now be calculated from Eqs. (5) and (6) using the experimentally measured scattered intensities from both the SNOM tip and the nanoantenna in the different configurations discussed above. To do that, we first perform a Gaussian fit in the images recorded with the EMCCD camera on each scattered spot produced by the tip and the antenna to extract the corresponding values of the scattered intensity. These values are then averaged over each scan line, resulting in 8 measurement points per scanning area. Figure 3 summarizes the obtained results. The dotted plots correspond to the decoupling coefficients of the SNOM tip for light propagating towards the base (green lines) and the apex of the nanotriangle (red lines). The average values are found to be $\gamma_{Pb} = 0.13 \pm 0.04$ and $\gamma_{Pa} = 0.12 \pm 0.03$. These similar values allow us to validate our hypothesis that the SNOM tip scatters the same fraction of light at any position on the DWG, which is independent of the light propagation direction. However, the solid curves, corresponding to the decoupling coefficients of the nanotriangle in both configurations, lead to the average values $\gamma_b = 0.66 \pm 0.07$ and $\gamma_a = 0.33 \pm 0.07$. As expected, the decoupling coefficients are strongly dependent on the light propagation direction through the DWG. The decoupling efficiency is thus much stronger for light propagating towards the base of the nanoantenna than in the opposite direction, proving the high directionality of our hybrid structure. This observation is confirmed by numerical simulations, performed in a broad spectral range and reported in Supplement 1, Fig. S1, that predict a decoupling ratio of 2.2 at $\lambda = 600$ nm.

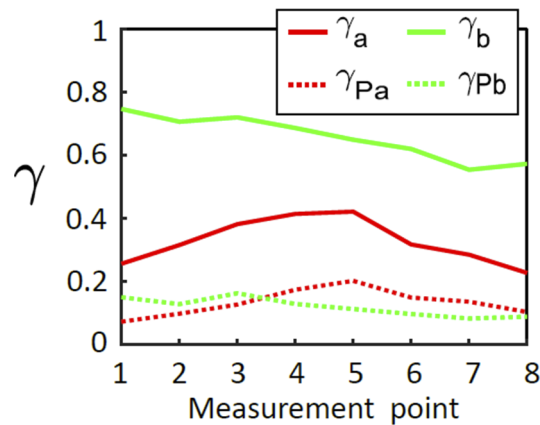


Fig. 3. Experimental values of the decoupling coefficients of the nanotriangle (solid plots) and the SNOM tip (dotted plots) calculated from the intensity maps. Green and red lines correspond to configurations where light is propagating towards the base and the apex of the nanotriangle respectively.

4. Numerical simulations: towards single-emitter coupling

Hybrid plasmonic/dielectric waveguides are particularly interesting when the question of coupling to the waveguide the light emitted by a fluorescent emitter is raised. As we will show with numerical simulations, the experimentally proven strong directionality of the light decoupled by our hybrid structure is confirmed when a single emitter interacts with the hybrid DWG. We perform Finite-Difference-Time-Domain (FDTD) simulations to investigate the coupling into the DWG of the radiation emitted by a dipole emitter interacting with the nanotriangle. We expect to observe a similar directionality of the light from the dipole coupled by the nanoantenna into the DWG as the decoupled light observed experimentally. Figures 4(a) and 4(b) present a schematic of our simulated structure, where a gold nanotriangle (base = height = 500 nm, thickness = 50 nm)

is placed on a TiO₂ waveguide (width = 1 μm , thickness = 150 nm), with a 30 nm layer of SiO₂ in between (index of refraction $n = 1.46$). The waveguide is placed on a SiO₂ substrate. The index of refraction of the gold nanotriangle is taken from Yakubovsky et al. [28], and that of TiO₂ is taken from Sarkar et al. [29]. A dipole emitter, oriented along the X-axis, is placed 10 nm away from the apex along the X direction at a height of 55 nm on the top of the DWG. As demonstrated in previous studies [17,30,31] and tested by our simulations, this configuration has shown to lead to efficient coupling into the DWG. Perfectly Matched Layer (PML) boundaries are used to absorb incident electromagnetic waves and avoid reflections. Two ‘frequency-domain field and power’ flat monitors (schematized by the red lines M₁ and M₂ on Figs. 4(a)-4(b) are placed along the X axis and perpendicular to the DWG, 10 μm away from the nanotriangle to avoid simulation artifacts (see Supplement 1, section 2 for a detailed explanation). These monitors are used to record the optical power (P_i) and allow us to extract the fraction of light injected in the DWG on both sides. A third monitor (a cube of 10 nm side) is placed around the dipole to detect the emitted power in its specific environment (P_E). This serves as a reference to which the light coupled into the waveguide on each side of the triangle is compared. The corresponding fraction of coupled light is thus calculated as $T_i = P_i/P_E$. The results are shown in Fig. 4(c). The green plot represents the fraction of coupled light measured by the monitor M₁ located at the side of the base of the nanotriangle (T_1). We can clearly observe that up to 30% of the power radiated by the dipole is coupled to the DWG at the base of the nanotriangle, and that this efficient coupling is achieved over a large wavelength range (600 nm – 800 nm). This is made possible by the plasmonic nature and the shape of the nanoantenna, which increases the coupling efficiency into the DWG, and by the dielectric nature of the DWG which allows the propagation

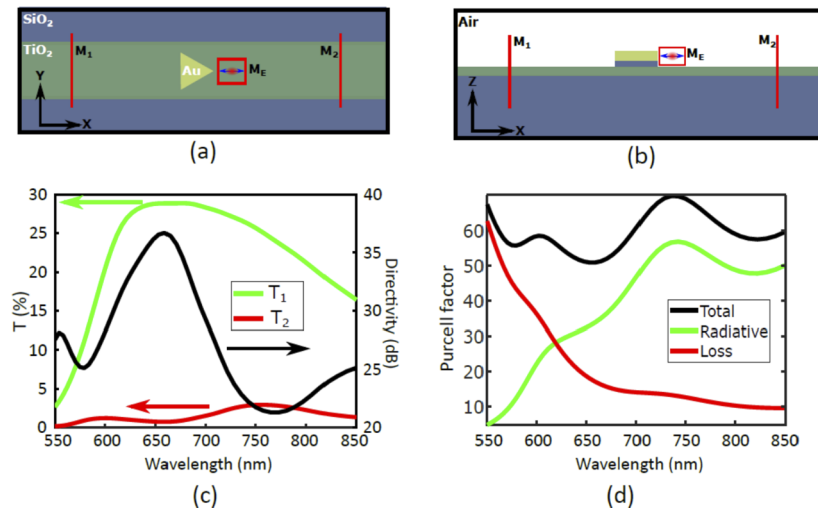


Fig. 4. (a) Simulation sketch top view ((b) cross view) of a dipole emitter placed at the apex of the nanotriangle and oriented along the X-axis. Red lines and square model the monitors M_{1,2} used for the simulation. The SiO₂ layer (thickness 30 nm) and the coverslip are schematized in blue, the TiO₂ DWG (width = 1 μm , thickness = 150 nm) in green and the gold nanoantenna (base = height = 500 nm) in yellow. (c) Simulation results corresponding to the configuration described in (a) for M_{1,2} placed 10 μm away from the nanotriangle along the X-axis. Green and red plots correspond to the fraction of light coupled in the DWG when the light propagates towards the base and the apex of the nanotriangle respectively. Black plot: directivity D of the injection in the DWG. (d) Purcell factor (black curve), radiative (green curve) and non-radiative (red curve) components computed for the configuration described in (a).

of guided light over long distances with minimum losses [32]. This agrees with the fact that, when a nanotriangle is illuminated through the DWG from the base-side, a hotspot characterized by high field concentration is produced at the apex, a phenomenon which does not occur in the reverse situation [16,17]. Therefore a dipole placed close to the apex of the nanotriangle will couple to the DWG via the nanotriangle more efficiently than a dipole placed at the base. This is shown through a numerical comparative study of the two scenarios reported in Supplement 1, Fig. S3. We also note that the maximum coupling of 30% in the DWG is a significant enhancement in comparison with the situation in which the dipole radiates in the absence of the nanotriangle where a coupling of about 4% is only achieved.

On the other hand, we notice that only a tiny percentage of the power radiated by the dipole is coupled in the DWG on the opposite direction (T_2). Numerical values of the directivity $D = 10 \cdot \log(T_1/T_2)$ are shown by the black line in Fig. 4(c). It can be clearly observed that the directivity has a maximum at 660 nm, which corresponds to the optimization wavelength.

In order to account for the efficiency of the device, we computed the Purcell factor which characterized the enhancement of the Local Density of States (LDOS) at the position of the dipole. The results of the computation for the total Purcell factor and its radiative and non-radiative contributions are shown in Fig. 4(d). At $\lambda = 600$ nm the Purcell factor is around 55 with a balanced contribution of the radiative and non-radiative components.

5. Conclusion

In this work, we developed a hybrid optical system consisting of a gold nanotriangle deposited on a TiO_2 dielectric waveguide. The importance of this hybrid structure is that it makes use of both the plasmonic nature of the nanoantenna and the dielectric nature of the waveguide to attain high coupling efficiency and directivity, achieving strong confinement of the incident light and propagation to large distances with small losses. The structure was first characterized experimentally by comparing the intensity scattered by the nanoantenna and a SNOM tip, as a function of the direction of the injection of light in the DWG. This allowed us to extract the decoupling efficiency of the nanotriangle and demonstrate its directionality. FDTD simulations were carried out to characterize the coupling with a single dipole emitter. It was shown that the nanotriangle couples light more efficiently towards its base, demonstrating directivity of almost 40 dB. The strong dependence of the resonance wavelength and the directivity on the dimensions of the nanoantenna suggest that different types of hybrid structures with different sizes, shapes and materials can be studied aiming to reach higher coupling efficiencies. Moreover, our experimental and modeling work highlights the ability of this hybrid photonic device to perform energy transfer, over large distances, between two quantum emitters. To this aim, two nanoantennas could be fabricated on the same DWG (see Fig. 1(b)), one to optimize the coupling of an emitter to the DWG and the other to couple the light in the DWG to a receiver. A future development will be to place single dipole emitters precisely at the electromagnetic hot spots of the antennas which should be feasible by means of photopolymerization methods [26,27,31,33,34]. In this way one should be able to experimentally demonstrate the coupling between two quantum emitters located far apart on a DWG. This work paves the way to achieve efficient energy transfer over considerably large distances on an integrated optical device, which can lead to promising improvement in the field of quantum information processing.

Funding. Ville de Paris (Emergences de la Ville de Paris 2015); LABEX WIFI (ANR-10-LABX-24, ANR-10-IDEX-0001-02 PSL); Conseil régional du Grand Est; FEDER.

Acknowledgments. Samples were fabricated using the Nanomat' platform partly funded by the Grand Est region and the FEDER funds.

Disclosures. The authors declare no conflicts of interest.

Data availability. Data underlying the results presented in this paper are not publicly available at this time but may be obtained from the authors upon reasonable request.

Supplemental document. See [Supplement 1](#) for supporting content.

References

1. C. Sun, M. T. Wade, Y. Lee, J. S. Orcutt, L. Alloatti, M. S. Georgas, A. S. Waterman, J. M. Shainline, R. R. Avizienis, S. Lin, B. R. Moss, R. Kumar, F. Pavanello, A.H. Atabaki, H.M. Cook, A.J. Ou, J.C. Leu, Y. Chen, K. Asanovic, R. J. Ram, M.A. Popovic, and V.M. Stojanovic, "Single-chip microprocessor that communicates directly using light," *Nature* **528**(7583), 534–538 (2015).
2. I. A. Young, E. Mohammed, J. T. Liao, A. M. Kern, S. Palermo, B. A. Block, M. R. Reshotko, and P. L. Chang, "Optical I/O technology for tera-scale computing," *IEEE J. Solid-State Circuits* **45**(1), 235–248 (2010).
3. M. J. Koblinsky, B. A. Block, J.-F. Zheng, B. C. Barnett, E. Mohammed, M. Reshotko, F. Robertson, S. List, I. Young, and K. Cadien, "On-Chip Optical Interconnects," *Intel Technology Journal* **8**(2), 129–141 (2004).
4. J. L. O'Brien, A. Furusawa, and J. Vučković, "Photonic quantum technologies," *Nat. Photonics* **3**(12), 687–695 (2009).
5. D. E. Chang, V. Vuletić, and M. D. Lukin, "Quantum nonlinear optics—photon by photon," *Nat. Photonics* **8**(9), 685–694 (2014).
6. T. E. Northup and R. Blatt, "Quantum information transfer using photons," *Nat. Photonics* **8**(5), 356–363 (2014).
7. J. Wang, S. Paesani, Y. Ding, R. Santagati, P. Skrzypczyk, A. Salavrakos, J. Tura, R. Augustiak, L. Mančinska, D. Bacco, D. Bonneau, J. W. Silverstone, Q. Gong, A. Acin, K. Rottwitt, L. K. Oxenlowe, J. L. O'Brien, A. Laing, and M. G. Thompson, "Multidimensional quantum entanglement with large-scale integrated optics," *Science* **360**(6386), 285–291 (2018).
8. D. Wang, H. Kelkar, D. Martin-Cano, D. Rattenbacher, A. Shkarin, T. Utikal, S. Götzinger, and V. Sandoghdar, "Turning a molecule into a coherent two-level quantum system," *Nat. Phys.* **15**(5), 483–489 (2019).
9. I. Aharonovich, D. Englund, and M. Toth, "Solid-state single-photon emitters," *Nat. Photonics* **10**(10), 631–641 (2016).
10. E. Knill, R. Laflamme, and G. J. Milburn, "A scheme for efficient quantum computation with linear optics," *Nature* **409**(6816), 46–52 (2001).
11. P. Lodahl, "Quantum-dot based photonic quantum networks," *Quantum Sci. Technol.* **3**(1), 013001 (2018).
12. L. Vertchenko, N. Akopian, and A. V. Lavrinenko, "Epsilon-Near-Zero Grids for On-chip Quantum Networks," *Sci. Rep.* **9**(1), 6053–6057 (2019).
13. D. Bouchet, D. Cao, R. Carminati, Y. De Wilde, and V. Krachmalnicoff, "Long-range plasmon-assisted energy transfer between fluorescent emitters," *Phys. Rev. Lett.* **116**(3), 037401 (2016).
14. D. Bouchet, E. Lhuillier, S. Ithurria, A. Gulinnati, I. Rech, R. Carminati, Y. De Wilde, and V. Krachmalnicoff, "Correlated blinking of fluorescent emitters mediated by single plasmons," *Phys. Rev. A* **95**(3), 033828 (2017).
15. X. He, L. Yang, and T. Yang, "Optical nanofocusing by tapering coupled photonic-plasmonic waveguides," *Opt. Express* **19**(14), 12865–12872 (2011).
16. Y. Luo, M. Chamanzar, and A. Adibi, "Compact on-chip plasmonic light concentration based on a hybrid photonic-plasmonic structure," *Opt. Express, OE* **21**(2), 1898–1910 (2013).
17. Y. Luo, M. Chamanzar, A. Apuzzo, R. Salas-Montiel, K. N. Nguyen, S. Blaize, and A. Adibi, "On-chip hybrid photonic-plasmonic light concentrator for nanofocusing in an integrated silicon photonics platform," *Nano Lett.* **15**(2), 849–856 (2015).
18. J. B. Madrigal, R. Tellez-Limon, F. Gardillou, D. Barbier, W. Geng, C. Couteau, R. Salas-Montiel, and S. Blaize, "Hybrid integrated optical waveguides in glass for enhanced visible photoluminescence of nanoemitters," *Appl. Opt.* **55**(36), 10263–10268 (2016).
19. D. Vercruyse, P. Neutens, L. Lagae, N. Verellen, and P. Van Dorpe, "Single asymmetric plasmonic antenna as a directional coupler to a dielectric waveguide," *ACS Photonics* **4**(6), 1398–1402 (2017).
20. D. Vercruyse, Y. Sonnefraud, N. Verellen, F. B. Fuchs, G. Di Martino, L. Lagae, V. V. Moshchalkov, S. A. Maier, and P. Van Dorpe, "Unidirectional Side Scattering of Light by a Single-Element Nanoantenna," *Nano Lett.* **13**(8), 3843–3849 (2013).
21. J. Li, N. Verellen, D. Vercruyse, T. Bearda, L. Lagae, and P. Van Dorpe, "All-Dielectric Antenna Wavelength Router with Bidirectional Scattering of Visible Light," *Nano Lett.* **16**(7), 4396–4403 (2016).
22. D. Vercruyse, X. Zheng, Y. Sonnefraud, N. Verellen, G. Di Martino, L. Lagae, G. A. Vandenbosch, V. V. Moshchalkov, S. A. Maier, and P. Van Dorpe, "Directional fluorescence emission by individual V-antennas explained by mode expansion," *ACS Nano* **8**(8), 8232–8241 (2014).
23. F. Bernal Arango, A. Kwadrin, and A. F. Koenderink, "Plasmonic Antennas Hybridized with Dielectric Waveguides," *ACS Nano* **6**(11), 10156–10167 (2012).
24. V. Loo, G. Blanquer, M. Joos, Q. Glorieux, Y. De Wilde, and V. Krachmalnicoff, "Imaging light scattered by a subwavelength nanofiber, from near field to far field," *Opt. Express* **27**(2), 350–357 (2019).
25. L. Aigouy, P. Lalanne, J. P. Hugonin, G. Julié, V. Mathet, and M. Mortier, "Near-field analysis of surface waves launched at nanoslit apertures," *Phys. Rev. Lett.* **98**(15), 153902 (2007).
26. X. Xu, A. Broussier, T. Ritacco, M. Nahra, F. Geoffroy, A. Issa, S. Jradi, R. Bachelot, C. Couteau, and S. Blaize, "Towards the integration of nanoemitters by direct laser writing on optical glass waveguides," *Photonics Res.* **8**(9), 1541–1550 (2020).

27. C. Deeb, R. Bachelot, J. Plain, A.-L. Baudrion, S. Jradi, A. Bouhelier, O. Soppera, P. K. Jain, L. Huang, C. Ecoffet, L. Balan, and P. Royer, "Quantitative analysis of localized surface plasmons based on molecular probing," *ACS Nano* **4**(8), 4579–4586 (2010).
28. D. I. Yakubovsky, A. V. Arsenin, Y. V. Stebunov, D. Y. Fedyanin, and V. S. Volkov, "Optical constants and structural properties of thin gold films," *Opt. Express* **25**(21), 25574–25587 (2017).
29. S. Sarkar, V. Gupta, M. Kumar, J. Schubert, P. T. Probst, J. Joseph, and T. A. König, "Hybridized guided-mode resonances via colloidal plasmonic self-assembled grating," *ACS Appl. Mater. Interfaces* **11**(14), 13752–13760 (2019).
30. R. Salas-Montiel, M. Berthel, J. Beltran-Madrigal, S. Huant, A. Drezet, and S. Blaize, "Local density of electromagnetic states in plasmonic nanotapers: spatial resolution limits with nitrogen-vacancy centers in diamond nanospheres," *Nanotechnology* **28**(20), 205207 (2017).
31. A. B. Vasista and G. P. Kumar, "Quantum emitter coupled to plasmonic nanotriangle: Spatially dependent emission and thermal mapping," *Opt. Commun.* **381**, 227–233 (2016).
32. J. Beltran Madrigal, "Integration of a single photon source on a planar dielectric waveguide," Doctoral dissertation, Université de technologie de Troyes (2017).
33. A. Broussier, A. Issa, L. O. Le Cunff, T. H. Nguyen, X. Q. Dinh, S. Blaize, J. Plain, S. Jradi, C. Couteau, and R. Bachelot, "Hybrid plasmonic nanosystem with controlled position of nanoemitters," *Appl. Phys. Lett.* **114**(16), 163106 (2019).
34. D. Ge, S. Marguet, A. Issa, S. Jradi, T. H. Nguyen, M. Nahra, J. Béal, R. Deturche, H. Chen, S. Blaize, J. Plain, C. Fiorini, L. Douillard, O. Soppera, X. Q. Dinh, C. Dang, X. Yang, T. Xu, B. Wei, X. W. Sun, C. Couteau, and R. Bachelot, "Hybrid plasmonic nano-emitters with controlled single quantum emitter positioning on the local excitation field," *Nat. Commun.* **11**(1), 1–11 (2020).